Research Article

Hatem Gasmi, Akintayo Oladimeji Akindele, Adebowale Martins Obalalu, Abdulazeez Adebayo Usman, Umair Khan*, Yalcin Yilmaz, Musilimu Taiwo, Syed Modassir Hussain, and Neelima Nizampatnam

Electromagnetic control and heat transfer enhancement in exothermic reactions experiencing current density: The study preventing thermal explosions in reactive flow

https://doi.org/10.1515/arh-2024-0020
received August 10, 2024; accepted September 29, 2024

Abstract: Thermal explosions in reactive flows present an important risk to industrial engineering systems, where uncontrolled exothermic reactions can compromise safety and operational integrity. This study investigates the theoretical solutions related to thermal runaway and heat transport in a branch-chain bifurcation scenario influenced by hydromagnetic Powell–Eyring fluid flow. By incorporating factors such as current density and variable properties, we aim to enhance the safety, reliability, and efficiency of industrial operations, thus contributing to the development of more robust and sustainable systems. Notably, the fluid is characterized by active exothermic behavior under bimolecular kinetics, challenging traditional material assumptions. Utilizing a spectral collocation scheme alongside exact solutions, we derive critical parameters, including flow velocity, current density, bifurcation branch-chain criticality, entropy generation rate, and heat propagation. Our findings reveal that increased electric field conductivity significantly enhances the current density along the channel walls, driven by the combined effects of the Frank–Kamenetskii term and electric field loading. Furthermore, understanding thermal explosions and branched-chain reactions is essential for preventing engine failures, underscoring the practical implications of this research in industrial contexts.

Keywords: Powell, Eyring fluid flow, thermal explosions, thermal runaway, chemical kinetics, entropy generation

*** Corresponding author: Umair Khan**, Department of Mathematics, Faculty of Science, Sakarya University, Serdivan/Sakarya, 54050, Turkey; Department of Computer Science and Mathematics, Lebanese American University, Byblos, Lebanon; Department of Mechanics and Mathematics, Western Caspian University, Baku, 1001, Azerbaijan, e-mail: umairkhan@sakarya.edu.tr
Hatem Gasmi: Department of Civil Engineering, College of Engineering, University of Hail, Hail, Saudi Arabia, e-mail: gasmi_hatem@yahoo.fr
Akintayo Oladimeji Akindele: Department of Pure and Applied Mathematics, Ladoke Akintola University of Technology, Ogbomoso, Oyo State, Nigeria, e-mail: aoakindele21@lautech.edu.ng
Adebowale Martins Obalalu: Department of Mathematics and Statistics, Kwara State University, Malete, Nigeria, e-mail: adebowale.obalalu17@kwasu.edu.ng
Abdulazeez Adebayo Usman: Department of Physical and Chemical Sciences, Federal University of Health Sciences Ila-Orangun, Ila-Orangun, Nigeria, e-mail: abdulazeez.usman@fuhsi.edu.ng
Yalcin Yilmaz: Department of Mathematics, Faculty of Science, Sakarya University, Serdivan/Sakarya, 54050, Turkey, e-mail: yalciny@sakarya.edu.tr
Musilimu Taiwo: Department of Physical and Chemical Sciences, Federal University of Health Sciences Ila-Orangun, Ila-Orangun, Nigeria, e-mail: nigeria.musilimu.taiwo@fuhsi.edu.ng
Syed Modassir Hussain: Department of Mathematics, Faculty of Science, Islamic University of Madinah, Madinah, 42351, Saudi Arabia, e-mail: syed.hussain@iu.edu.sa
Neelima Nizampatnam: Department of Electronics and Communication, Amrita School of Engineering, Amrita Vishwa Vidyapeetham, Bangalore, India, e-mail: n_neelima@blr.amrita.edu

Nomenclature

x^*, y^*	Cartesian coordinates
h	Channel width, m
a^*	Fluid flow velocity, m s^{-1}
B_0	Magnetic field strength, Wb m^{-2}
T^*	Dimensional fluid temperature, K
T_0^*	Fluid temperature at the wall, K
ς_0	Injection/suction
μ	Fluid viscosity, kg m^{-1} s^{-1}
β	Thermal expansion coefficient, K^{-1}
C_p	Specific heat capacity, J kg^{-1} K^{-1}
ν	Vibration frequency
r_1, r_2	Coefficient of Navier slip

Q	Heat reaction term, W
A	Constant reaction rate
Gr	Thermal Grashof number
ϱ	Powell–Eyring parameter
a	Variable thermal conductivity
ϵ	Activation energy
ϑ	Dimensionless temperature
g	Gravitational force, m s^{-2}
Ha	Hartmann number
σ_0	Electrical conductivity
R	Universal gas constant
b	Electrical conductivity exponent
χ, ϖ	Fluid material constant
ρ	Density of the fluid, kg m^{-3}
E_M	Electrical field
Pr	Prandtl number
$k(T^*)$	Heat-dependent thermal conductivity, W m^{-1} K^{-1}
l	Planck number
g_1, g_2	Navier slip
C	Reactant species
k	Thermal conductivity, W m^{-1} K^{-1}
λ	Frank–Kamenetskii parameter
Br	Brinkman number
ϕ	Electric field loading
H	Dimensionless velocity

1 Introduction

According to the laws of thermodynamics, entropy generation serves as a metric for the inherent inefficiency present in all energy conversion processes in the real world. Entropy generation is particularly useful in the context of heat engines, refrigeration systems, and other thermodynamic processes. Therefore, engineers can analyze and calculate the energy losses in the system they are working with by using the idea of entropy generation [1]. Two cycles govern the entropy generation, which are the Carnot and Otto cycles; the most effective thermodynamic cycle, with zero entropy formation under perfect conditions, is the Carnot cycle. Both adiabatic and isothermal processes make up this cycle. Because it denotes the maximum efficiency that an engine may attain, it is an essential thermodynamic benchmark. However, in practice, no practical engine can reach the Carnot efficiency because of irreversibilities like heat losses and friction, which constantly generate some entropy [2]. Another excellent study for entropy formation is the Otto cycle, which serves as a realistic model for gasoline engines. Because entropy is generated during combustion and exhaust processes, when heat transfer over limited temperature differences occurs, this cycle is intrinsically irreversible [3]. As a result, they may modify their designs to minimize these losses, increasing the effectiveness of the regime. According to Nasrin and Alim [4], the non-equilibrium flow produced by boundary conditions (BCs) is what generates entropy in the flow field. Entropy is generated during the convection process as a result of irreversibility brought on by the heat transfer phenomenon and friction in the fluid movement. Many studies have been carried out on entropy generation based on different flow models: Sharma et al. [5] considered a flow model with an electromagnet-hydrodynamic Jeffrey nanofluid flow. This research lays more emphasis on solar radiation, which is an increasing function of the temperature distribution. Ullah et al. [6] worked on a flow model that includes a magnetohydrodynamic (MHD) hybrid nanofluid considering moving plates. The entropy generation studied in this research affects the magnetic term positively due to the greater resistance of the fluid flow that is produced by the Lorentz force, leading to higher entropy production. Furthermore, Obalalu et al. [7] addressed entropy generation on a Casson fluid flow model; although the numerical aspect was the focus point, the effects of some physical parameters like the radiation parameter and Eckert number were well explained on the entropy generation profile. The flow model that involves the variable properties, exponential porous fins, radiation, and heat generation was analyzed by Din et al. [8] using the shooting technique as the numerical method. One of their observations revealed that the temperature ratio and the entropy generation profile are directly promotional to each other. Favas and Jilani [9] also considered entropy generation on a flow model that involves variable properties and heat generation, but they used a different numerical method called a line-by-line Gauss–Seidel iteration method, and their result includes the entropy generation profile also increasing the temperature ratio. In addition, Rikitu and Makinde [10] examined the second law and heat transfer analysis in a non-Newtonian (Eyring-Powell) nanofluid flow past an inclined microchannel with Lorentz forces and heat generation effects.

The field of MHD, also known as magnetofluid dynamics or hydromagnetics, involves the examination of the performance of fluids that conduct electricity [11,12]. MHD plays a crucial role in analyzing the entropy generation of a system, particularly in heat transfer. Abbas et al. [12] studied MHD dusty flow by adding three types of nanoparticles into the model and taking into consideration a non-linear heat source term. Waqas et al. [13] studied the non-Newtonian Eyring–Powell fluid model MHD flow under the influence of solar radiation and generalized Arrhenius kinetics. The method of homotopy analysis was used by Lone et al. [14] to solve a model involving MHD blood-based ternary hybrid nanofluid flow with velocity slip conditions. MHD involved in the flow causes the velocity profile to retardate while the thermal

field gives an increasing function of the MHD. Previous studies [15–20] show further research on entropy generation and MHD flows.

Non-Newtonian fluids are characterized by their deviation from Newton's law of viscosity. Moreover, the shear stress in non-Newtonian fluids is not directly proportional to the velocity gradient as defined by Newton's equation of viscosity [21]. Examples of non-Newtonian fluids are paint, toothpaste, and ketchup paste; these fluids exhibit a drop in viscosity and an increase in velocity when subjected to force or pressure. That being said, not all non-Newtonian fluids display these qualities [22]. The Eyring–Powell fluid is a non-Newtonian fluid that Eyring and Powell discovered in the year 1944. It exhibits both thixotropic and shear thinning (pseudo-plastic) characteristics. The Eyring–Powell fluid is used in many different businesses and research domains, including the production of pharmaceuticals, food, cosmetics, paint, and coating companies, oil and gas, and polymer processing. To have a thorough grasp of these fluids and their diverse uses, it is essential to investigate the behavior of the Eyring–Powell fluid under various situations. According to earlier studies, the importance of the Eyring–Powell fluid and its uses in the applied sciences and other technological processes cannot be overstated. Hussain et al. [23] examined the MHD ternary hybrid nanofluid flow past a stretching sheet subject to convective boundary conditions. The resultant ODE was elaborated numerically using a spectral quasi-linearization scheme. The Eyring–Powell model with MHD and bi-convective heating is numerically investigated by Iqbal et al. [24] using the shooting technique, taking into account gyrotactic microorganisms. The temperature distribution is significantly increased as a result of the addition of MHD and convective heating to the Eyring–Powell model. The Eyring–Powell model was also utilized by Khan et al. [25] to study the electromagnetic effect in an axisymmetric channel. The homotopy perturbation method is used to calculate against the resulting equations. The results showed that the temperature distribution is exactly related to the electric and magnetic characteristics. Analysis by Vijatha and Bala Anki Reddy [26] made use of the homotopy perturbation approach to numerically solve the Cattaneo–Christov Eyring–Powell heat flow model. Allehiany et al. [27] analyzed a Cilia Eyring–Powell model with viscous dissipation and a vertical thermal channel using the Adomian decomposition approach. The investigation revealed that the Eyring–Powell parameter causes the flow to speed up by 10%. The MHD Eyring–Powell model was analyzed by Hussain and Mao [28] using a variable stretching sheet and Christov–Cattaneo heat flux. The resulting ODE was numerically solved using the shooting technique, and the result demonstrated that MHD had a positive effect on the temperature profile. The significance of mathematical simulation on a complicated form of heat radiation under the impact of entropy generation and some other dimensionless flow parameters was discussed by Nisar et al. [29] using the Powell–Eyring fluid model. A bioconvective Eyring–Powell nanofluid model was examined by Mondal and Pal [30] while taking into account variable characteristics and chemical reactions. The Runge–Kutta Felhberg technique was employed to numerically solve the model. Their findings showed that when the chemical reaction parameter increases, the concentration and microorganism density profiles decline.

An Eyring–Powell flow via a porous channel was explored by Nadeem et al. [31] using water as the base fluid and aluminum oxide nanoparticles. The investigation followed the use of the perturbation approach and showed a direct proportionality between the flow velocity and the Eyring–Powell parameter. A chemically reacting Eyring–Powell fluid flow was studied by Hussian et al. [32] while taking the radiation term and the density of motile microorganisms into account. The concentration distribution and microorganisms increase when the magnetic parameter and Biot's number increase. Ibrahim and Lamesse [33] quantitatively analyzed the Eyring–Powell nanofluid model over a stretched surface and convective heating using the finite elimination approach. Their findings revealed that the Eyring–Powell parameter significantly increases with increasing velocity profiles. Shah et al. [34] used the Runge–Kutta approach to adapt homogeneous and heterogeneous reactions to the Eyring–Powell nanofluid model, which was composed of microorganisms and variable characteristics. It was also noted that the Eyring–Powell parameter improved the flow movement.

The importance of studying thermal runaway cannot be overstated when it comes to Eyring–Powell reacting fluids, as a thermal explosion is a major threat when working with any reacting fluid. The primary goal of studying thermal runaway is to forecast the unsafe or critical state of a reacting fluid. When a thermally unstable reaction system demonstrates an uncontrollably increasing rate of reaction that quickly raises temperature and pressure, this is called a runaway chemical reaction. The effects are shown in Figure 1a. However, inappropriate response scaling, malfunctioning cooling or control systems, or accidental introduction of contaminants or unsuitable materials are some possible causes. The consequences for safety are enormous because these reactions can result in fires, toxic spills, or explosions, which pose serious risks to people's health, the environment, and properties. The recent work of Salawu et al. [35] studied the computational solution of thermal runaway on thermodynamic reacting couple stress fluid by considering slip conditions and variable properties. The analysis revealed that studying thermal explosion helps

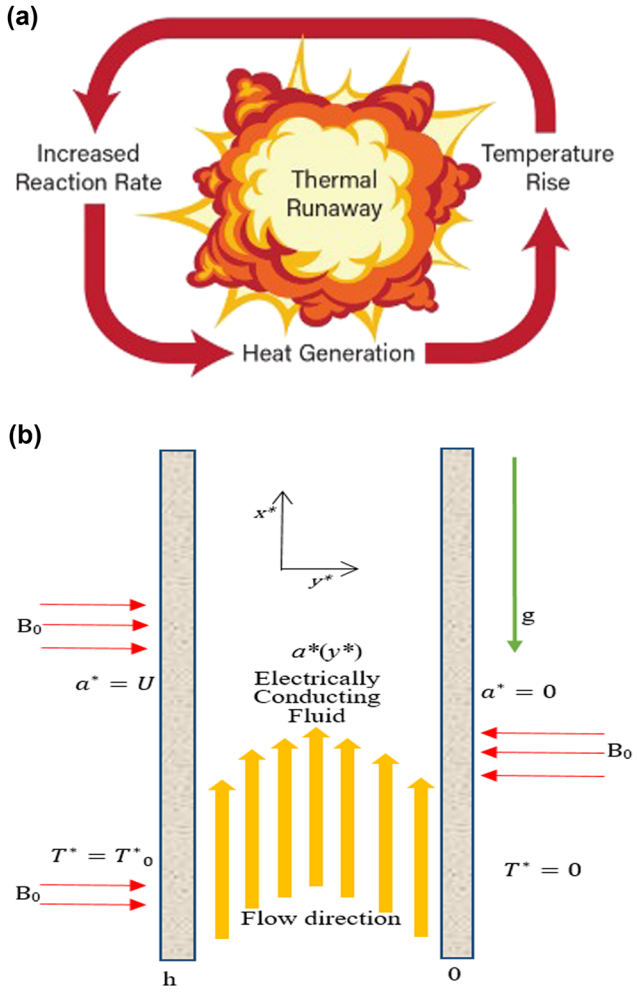

Figure 1: (a) A chain reaction analyzing the reasons behind thermal runaway. (b) Physical flow configuration.

improve the performance of a system and the design of multiple technological devices. The non-Darcy fully developed mixed convection in a porous medium channel with heat generation/absorption and the hydromagnetic effect was investigated by Chamkha [36].

1.1 The objective and novelty of the newly proposed model

This study aims to develop a theoretical model to prevent thermal explosions in reactive flows and improve heat transfer during exothermic reactions within the irreversibility process. It examines how Navier slip conditions and variable properties influence the heat transfer process. It further explores how the system performs under conditions of high thermodynamic equilibrium. It reveals that minimizing entropy production is vital for effectively managing energy in industrial engines. The newly proposed model offers a thorough analysis of bifurcation branches for criticality via employing the spectral collocation scheme (SCS). This investigation sheds light on the ignition and non-ignition phases of reactions involving the Powell–Eyring fluid, presenting novel findings. The study assumes the idealized behavior of the Powell–Eyring fluid, which may not fully represent the complexities of actual fluids in industrial environments.

1.2 Motivation and applications of the proposed study

The prevention of thermal explosions is motivated by key factors across different industrial sectors, including industrial systems design and operation, aerospace engineering, chemical reactors, combustion engines, and electric vehicles. This drive is crucial in ensuring safety and reliability in these diverse fields.

2 Description of the current model

This study investigates the exothermic reactive flow of a hydromagnetic over a vertical porous wall under bimolecular kinetics. The configuration of the reactive Powell–Eyring fluid and the schematic representation of the coordinate system are displayed in Figure 1b. In a non-isothermal setup, the flow walls are positioned at $y^* = [0, h]$, where y^* is perpendicular to the direction of the non-Newtonian flow along the x^*-axis. The analysis was based on the following assumptions in this case:

- The model is a steady and electrically conducting Eyring–Powell fluid flow.
- The hot fluid temperature is the term T^* for the lower plate of the channel and the ambient temperature T_0^* for the top plate.
- Thermal conductivity, the Frank–Kamenetskii term, heat-dependent dynamic viscosity, and magnetic field were also considered.

The electrical conductivity $\sigma(T^*)$ of the reactive fluid, which is dependent on heat, is defined as follows [35]:

$$\sigma(T^*) = \sigma_0 \left(\frac{E(T^* - T_0^*)}{RT_0^{*2}} \right)^b, \tag{1}$$

where σ_0 represents the electrical conductivity of the plate, and b denotes the electrical conductivity exponent. According to Algehyne et al. [20], the fluid model for the Cauchy Eyring–Powell stress tensor is as follows:

$$S_{ij} = \frac{1}{\varpi}\sinh^{-1}\left(\frac{1}{\chi}\frac{\partial a_i^*}{\partial x_j^*}\right) + \mu\frac{\partial a_i^*}{\partial x_j^*}, \tag{2}$$

where χ and ϖ represent the fluid material constants, while μ is the fluid viscosity coefficient:

$$\sinh^{-1}\left(\frac{1}{\chi}\frac{\partial a_i^*}{\partial x_j^*}\right) \cong \frac{1}{\chi}\frac{\partial a_i^*}{\partial x_j^*} - \frac{1}{6}\left(\frac{1}{\chi}\frac{\partial a_i^*}{\partial x_j^*}\right)^3. \tag{3}$$

According to the assumptions mentioned above, the governing equation for the velocity and heat balance of the reactive Powell–Eyring fluid with variable properties are given as follows [16,17]:

$$\begin{aligned}\varsigma_0\rho\frac{\mathrm{d}a^*}{\mathrm{d}y^*} &= -\frac{\mathrm{d}P^*}{\mathrm{d}x^*} + \left(\mu + \frac{1}{\varpi\chi}\right)\frac{\mathrm{d}^2a^*}{\mathrm{d}y^{*2}} - \frac{1}{2\varpi^3}\left(\frac{\mathrm{d}a^*}{\mathrm{d}y^*}\right)^2\frac{\mathrm{d}^2a^*}{\mathrm{d}y^{*2}} \\ &\quad - \sigma(T^*)B_0(B_0a^* + E_M) + g\beta(T^* - T_0^*),\end{aligned} \tag{4}$$

$$\begin{aligned}\varsigma_0\rho C_\mathrm{p}\frac{\mathrm{d}T^*}{\mathrm{d}y^*} &= k(T^*)\frac{\mathrm{d}^2T^*}{\mathrm{d}y^{*2}} + \frac{\mathrm{d}T^*}{\mathrm{d}y^*}\frac{\mathrm{d}k(T^*)}{\mathrm{d}y^*} \\ &\quad + QCA\left(\frac{\mathrm{KT}^*}{\nu l}\right)^n e^{\frac{E}{\mathrm{RT}^*}} + \sigma(T^*)B_0(B_0a^* + E_M)^2 \\ &\quad + \left(\frac{\mathrm{d}a^*}{\mathrm{d}y^*}\right)^2\left[\left(\mu + \frac{1}{\varpi\chi}\right) - \frac{1}{6\varpi\chi^3}\left(\frac{\mathrm{d}a^*}{\mathrm{d}y^*}\right)^2\right].\end{aligned} \tag{5}$$

The BCs are applied to the governing equations [19]:

$$\begin{aligned}&\frac{\mathrm{d}^2a^*(0)}{\mathrm{d}y^{*2}} = 0,\ a^*(0) = r_1\frac{\mathrm{d}a^*(0)}{\mathrm{d}y^*},\ T^*(0) = T_0, \\ &\frac{\mathrm{d}^2a^*(1)}{\mathrm{d}y^{*2}} = 0,\ a^*(1) = r_2\frac{\mathrm{d}a^*(1)}{\mathrm{d}y^*},\ \ T^*(1) = T_0^*.\end{aligned} \tag{6}$$

According to [23], the thermal conductivity $k(T^*)$ that varies exponentially are

$$k(T^*) = k_0\mathrm{e}^{a(T^* - T_0^*)}. \tag{7}$$

For certain liquids, such as air or water vapor, the term a can be positive; for other liquids, such as benzene, it can be negative. Equation (8) introduces the following quantities into equations (4)–(6) [37]:

$$\begin{aligned}&x = \frac{x^*}{h},\ U = \frac{a^*}{\varsigma_0},\ y = \frac{y^*}{h},\ P = \frac{P^*h}{\mu_0\varsigma_0},\ G = -\frac{\partial P}{\partial x}, \\ &\vartheta = \frac{E(T^* - T_0^*)}{\mathrm{RT}_0^{*2}},\ \mathrm{Ha} = \frac{h^2\sigma_0B_0^2}{\mu}, \\ &H = \frac{a^*}{U},\ r = \frac{h\varsigma_0}{\nu},\ \ g_1 = \frac{r_1}{h},\ g_2 = \frac{r_2}{h}.\end{aligned} \tag{8}$$

In dimensionless form, the primary equations and the BCs are as follows:

$$\begin{aligned}r\frac{\mathrm{d}H}{\mathrm{d}y} &= \frac{\mathrm{d}^2H}{\mathrm{d}y^2} + \alpha\frac{\mathrm{d}^2H}{\mathrm{d}y^2} - \varrho\alpha\left(\frac{\mathrm{d}H}{\mathrm{d}y}\right)^2\frac{\mathrm{d}^2H}{\mathrm{d}y^2} \\ &\quad - \mathrm{Ha}(\phi + H)\vartheta^b + G + \mathrm{Gr}\ \vartheta,\end{aligned} \tag{9}$$

$$\begin{aligned}r\mathrm{Pr}\frac{\mathrm{d}\vartheta}{\mathrm{d}y} &= \mathrm{e}^{a\vartheta}\frac{\mathrm{d}^2\vartheta}{\mathrm{d}y^2} + c\mathrm{e}^{a\vartheta}\left(\frac{\mathrm{d}\vartheta}{\mathrm{d}y}\right)^2 + \mathrm{Br}\left[\left(\frac{\mathrm{d}H}{\mathrm{d}y}\right)^2\left((1+\alpha) + \frac{\alpha\varrho}{3}\left(\frac{\mathrm{d}H}{\mathrm{d}y}\right)^2\right)\right. \\ &\quad \left. +\mathrm{Ha}(H+\phi)^2\vartheta^b\right] \\ &\quad + \lambda(1+\epsilon\vartheta)^n\mathrm{e}^{\frac{\vartheta}{1+\epsilon\vartheta}}.\end{aligned} \tag{10}$$

Together with the BCs,

$$\begin{aligned}&\frac{\mathrm{d}^2a^*(0)}{\mathrm{d}y^2} = 0,\ \ a^*(0) = g_1\frac{\mathrm{d}a^*(0)}{\mathrm{d}y},\ T^*(0) = 0, \\ &\frac{\mathrm{d}^2a^*(1)}{\mathrm{d}y^2} = 0,\ a^*(1) = g_2\frac{\mathrm{d}a^*(1)}{\mathrm{d}y},\ T^*(1) = 0.\end{aligned} \tag{11}$$

The control parameters and range values for the governing equation are listed in Table 1.

The coefficient of skin friction and Nusselt number are the quantities of engineering relevance and are defined as follows.

$$C_\mathrm{f} = \left.\frac{\partial H}{\partial y}\right|_{y=0,1},\quad \mathrm{Nu} = -\left.\frac{\partial\vartheta}{\partial y}\right|_{y=0,1}. \tag{12}$$

The current density for the reactive hydromagnetic fluid flow is described as

Table 1: Listings of the control parameters and range values for the governing equation

Parameters	Formulae	Symbols
Eyring–Powell fluid parameter	$\alpha = \frac{1}{\mu\varpi\chi}$	α
Hartmann number	$\mathrm{Ha} = \frac{h^2\sigma_0B_0^2}{\mu}$	Ha
Thermal Grashof number	$\mathrm{Gr} = \frac{g\beta h^2RT_0^*}{\mu U}$	Gr
Prandtl number	$\mathrm{Pr} = \frac{\mu c_\mathrm{p}}{k_0}$	Pr
Frank–Kamenetskii parameter	$\lambda = \frac{AQCh^2E}{Rk_0T_0^{*2}}\left(\frac{KT_0^*}{\nu l}\right)^n\mathrm{e}^{\frac{1}{\epsilon}}$	λ
Powell–Eyring parameter	$\varrho = \frac{U^2}{2\chi^2h^2}$	ϱ
Brinkman number	$\mathrm{Br} = \frac{\mu EU^2}{Rk_0T_0^{*2}}$	Br
Variable thermal conductivity	$a = \frac{aRT_0^{*2}}{E}$	a
Electric field loading	$\phi = \frac{E_M}{\mathrm{UB}_0}$	ϕ
Activation energy	$\epsilon = \frac{RT_0^*}{E}$	ϵ

$$I_{\mathrm{T}} = \int_0^1 (\phi + H)\vartheta^b \mathrm{d}y \quad \text{and} \quad I_{\mathrm{d}} = (\phi + H)\vartheta^b, \tag{13}$$

where I_{T} is the total generated current and I_{d} is the current density. It is vital to know that configuring a short circuit in the absence of a loading electric field, $\phi = 0$.

3 Evaluation of entropy generation

The concept of the first and second laws of thermodynamics is crucial for effectively studying and utilizing solar radiation mechanisms. According to Nadeem et al. [31], entropy represents the disruption of an orderly system and its surrounding environment, serving as a measure of irreversibility. It is challenging to convert the entire solar radiation into heat due to the presence of irreversibility, leading to a decrease in the overall efficiency of harnessing the sun's energy for work. In this study, the authors observed the level of disorder generated by the conversion of heat, friction of T-HNF, and mass transfer. Mathematically, entropy generation is expressed as [32]

$$I_{\mathrm{G}} = \frac{k(T^*)}{T_0^{*2}}\left(\frac{\mathrm{d}T^*}{\mathrm{d}y^*}\right)^2 + \frac{\mu}{T_0^*}\left[\left(1 + \frac{1}{\rho\varpi\chi}\right)\left(\frac{\mathrm{d}a^*}{\mathrm{d}y^*}\right)^2 - \frac{1}{6\rho\varpi\chi^3}\left(\frac{\mathrm{d}a^*}{\mathrm{d}y^*}\right)^4\right] + \frac{\sigma(T^*)B_0(B_0a^* + E_M)^2}{T_0^*}. \tag{14}$$

The first term in equation (14) describes the irreversibility of heat transmission, whereas the second and third terms in the equation reflect the irreversibility resulting from fluid friction and a magnetic field, respectively. The non-dimensional rate of entropy creation in equation (14) is obtained by using equation (8):

$$N_s = \frac{E^2h^2I_{\mathrm{G}}}{k_0R^2T_0^{*2}} = \mathrm{e}^{a\vartheta}\left(\frac{\mathrm{d}\vartheta}{\mathrm{d}y}\right)^2 + \frac{\mathrm{Br}}{\epsilon}\left[(1 + \alpha)\left(\frac{\mathrm{d}H}{\mathrm{d}y}\right)^2 - \frac{\alpha\delta}{3}\left(\frac{\mathrm{d}H}{\mathrm{d}y}\right)^4 + \mathrm{Ha}(\phi + H)^2\vartheta^b\right], \tag{15}$$

where

$$N_1 = \mathrm{e}^{a\vartheta}\left(\frac{\mathrm{d}\vartheta}{\mathrm{d}y}\right)^2 \text{ and } N_2 = \frac{\mathrm{Br}}{\epsilon}\left[(1 + \alpha)\left(\frac{\mathrm{d}H}{\mathrm{d}y}\right)^2 - \frac{\alpha\delta}{3}\left(\frac{\mathrm{d}H}{\mathrm{d}y}\right)^4 + \mathrm{Ha}(\phi + H)^2\vartheta^b\right], \tag{16}$$

Bejan number (Be) is defined as

$$\mathrm{Be} = \frac{N_1}{N_s} = \frac{1}{1 + \psi}, \tag{17}$$

where $\psi = \frac{N_2}{N_1}$, $N_s = N_2 + N_1$, and N_1 denotes the heat transfer irreversibility, N_2 denotes the magnetic field and fluid friction irreversibility, and ψ represents the irreversibility ratio. The range of Bejan number (Be) is $0 \le \mathrm{Be} \le 1$. When Be = 0, irreversibility results from fluid friction and magnetic fields, controlling the reactive flow system; however, when Be = 1, irreversibility results from heat transfer and heat differences.

4 Numerical procedure

4.1 A summary of SCS

SCT is a computational technique utilized in applied mathematics and scientific computing to solve differential equations (eigenvalue, Fourier series, ODEs, PDEs, etc.) and optimization problems [38]. The procedure involves approximating the solution of a differential equation by expressing it as a combination of basic functions. The basic functions selected are orthogonal, for instance, Legendre polynomials or Chebyshev polynomials. The fundamental idea of spectral collocation (SC) includes determining the weights of the basic functions that represent the solution in a specified range. This technique is usually engaged in SC to achieve precise solutions for differential equations.

The SC method entails the process of finding an estimated solution for a differential equation:

$$L(\chi(\tau)) + W(\tau) = 0, \text{ in domain, } D = [0, 1]. \tag{18}$$

Here, function $\chi(\tau)$ is an unknown function that depends on τ, $W(\tau)$ denotes the source term, and L is the differential operator. Furthermore, the given solution must meet the BCs to be considered as an appropriate approximation:

$$\chi(\tau) = \sum_{m-0}^{p} w_m Q_m \ (2\tau - 1), \tag{19}$$

where w_m are coefficients of unknown constants and functions. $Q_m(2\tau - 1)$ are shifted Chebyshev base functions, rescaled from the interval [−1, 1] to [0, 1]. To determine the values of the w_m, equation (19) is replaced with equation (18), producing the residual error $R_\chi(\tau, w_m)$:

$$\text{for } \pi(\tau - \tau_m) = \begin{cases} 1, & \tau = \tau_m, \\ 0, & \text{otherwise}, \end{cases} \tag{20}$$

$$\int_0^1 R_\chi((\tau, w_m)\pi(\tau - \tau_m)\mathrm{d}\tau = R_\chi(\tau, w_m) = 0,$$

$$\text{for } m = 1, 2, \ldots N - 1$$

The shifted Gauss–Lobatto points are represented via $\tau_m = \frac{1}{2}\left(1 - \cos\left(\frac{m\delta}{N}\right)\right)$. This formula describes the specific positions of these points.

4.2 Application of SCS

The solutions for $H\ (\eta)$ and $\vartheta\ (\eta)$ are as follows:

$$H(\eta) = \sum_{m-0}^{p} c_m Q_m(2\eta - 1)$$
$$\text{and} \tag{21}$$
$$\partial(\eta) = \sum_{m-0}^{p} d_m Q_m(2\eta - 1)$$

To determine the values of the constant coefficients that are unknown, we can replace expression (19) with equation (6) to satisfy the BCs.

$$\begin{aligned}
&\left[\sum_{m=0}^{p} c_m Q_m(2\eta - 1)\right]_{\tau=0} = 0,\\
&\left[\sum_{m=0}^{p} d_m Q_m(2\eta - 1)\right]_{\tau=0} = 0,\\
&\left[\sum_{m=0}^{p} c_m Q_m(2\eta - 1)\right]_{\tau=1} = 0,\\
&\left[\sum_{m=0}^{p} d_m Q_m(2\eta - 1)\right]_{\tau=1} = 0.
\end{aligned} \tag{22}$$

Equation (18) is inserted into equations (9) and (10), producing the residues $R_H(\eta, a_i)$ and $R_\vartheta(\eta, c_m, d_m)$. Subsequently, the collocation method is employed to minimize these residues, as outlined in the following:

$$\begin{aligned}
&\int_0^1 R_H \gamma(\tau - \tau_m)\mathrm{d}\tau = R_H(\tau_m, c_m) = 0,\\
&\text{for } m = 1,\ 2, \ldots N - 1,\\
&\int_0^1 R_\vartheta \gamma(\tau - \tau_m)\mathrm{d}\tau = R_\vartheta(\tau_m, c_m, d_m) = 0,\\
&\text{for } m = 1,\ 2, \ldots N - 3.
\end{aligned} \tag{23}$$

The system of algebraic equations, derived from equations (22) and (23), consists of $2N + 2$ equations involving $2N + 2$ unknown constants (c_m, d_m). These equations are then solved utilizing the Newton method using the symbolic computational software MATHEMATICA 11.3.

4.3 Comparison between solutions of exact and adomian decomposition procedure

The method's consistency and accuracy are validated and presented in Table 2. The comparison of results between the exact findings and previous research is presented in Table 1. The SCS reveals favorable outcomes when compared to the results obtained through the exact ADM. This comparison showcases the effectiveness of the SCS in generating reliable outcomes. The SCS aligned well with the other solution methods, exhibiting an absolute error order of 10^{-7}.

5 Results and interpretations

This section uses graphical illustrations to visually depict how different control parameters affect velocity and temperature profiles. The ranges of controlling parameters are magnetic field (M = 0.1, 0.2, 0.3, 0.4), viscosity (α = 0.3, 0.5, 0.7, 0.9), Powell–Eyring (ϱ = 0.2, 0.3, 0.5, 0.7), pressure gradient (G = 1, 3, 5, 7), Frank–Kamenetskii (λ = 0.2, 0.5, 0.7, 1.0), electric field loading (ϕ = 0.2, 0.3, 0.7, 1.0), and Brinkman number (Br = 0.1, 0.2, 0.3, 0.4).

5.1 Magnetic field parameter (M)

The influence of the magnetic field parameter (M) on the fluid flow of HHF and a T-HHF is thoroughly studied. The observation made in Figure 2a shows a decline in speed

Table 2: Comparison of the computed values of the exact solution and existing work

ω	ω_{exact}	ω_{ADM}, results of [19]	ω_S	Absolute error
0.0	0.00303054	0.00303070	0.00303067	1.0012×10^{-7}
0.1	0.00598827	0.00598858	0.00598851	1.6750×10^{-7}
0.2	0.00854151	0.00854196	0.00854182	2.3164×10^{-7}
0.3	0.01037320	0.01037370	0.01037361	2.7968×10^{-7}
0.4	0.01125880	0.01125950	0.01125933	3.6802×10^{-7}
0.5	0.01106440	0.01106510	0.01106497	4.2994×10^{-7}
0.6	0.00974517	0.00974577	0.000974568	4.3776×10^{-7}
0.7	0.00734506	0.00734554	0.00734550	4.4422×10^{-7}
0.8	0.00399756	0.00399783	0.00399779	2.2145×10^{-7}
0.9	−0.00007304	−0.00007305	−0.00007305	9.1365×10^{-8}
1.0	−0.00454921	−0.00454955	−0.00454947	2.4321×10^{-7}

distribution as the M increases. Figure 2a exhibits three curves corresponding to varying M values (0.1, 0.2, 0.3, and 0.4). With an improvement in the magnetic field, the curves display a reduction in the value, signifying a diminution in the speed distribution as the M value increases; the physical reason behind this effect is ascribed to a force identified as the Lorentz force. When a charged particle moves within a magnetic field, it experiences the inspiration of the Lorentz force (LF).

5.2 Viscosity parameter (α)

Viscosity refers to how much a liquid resists deformation or flow. A liquid with large viscosity is thicker and more resistant, while a liquid with low viscosity is thinner and flows more easily. The effect of the α parameter on the fluid flow is shown in Figure 2b. A larger α leads to improved viscosity, resulting in a slower fluid flow. The reason for this is that the viscosity of various liquids varies depending on the temperature. Once the temperature of most liquids increases, their viscidness tends to reduce. Consequently, a liquid that is warmed up will have an easier flow. The influence is larger toward the center of the channel and has a smaller impact closer to the channel plates.

5.3 Powell–Eyring parameter (ϱ)

The Powell–Eyring liquid model employs ϱ to illustrate the rheological features of non-Newtonian liquids. $H(\eta)$ increases with increasing values of ϱ, as shown in Figure 2c. The improvement observed can be attributed to the decrease in fluid viscosity, as it has an inverse relationship with fluid viscosity.

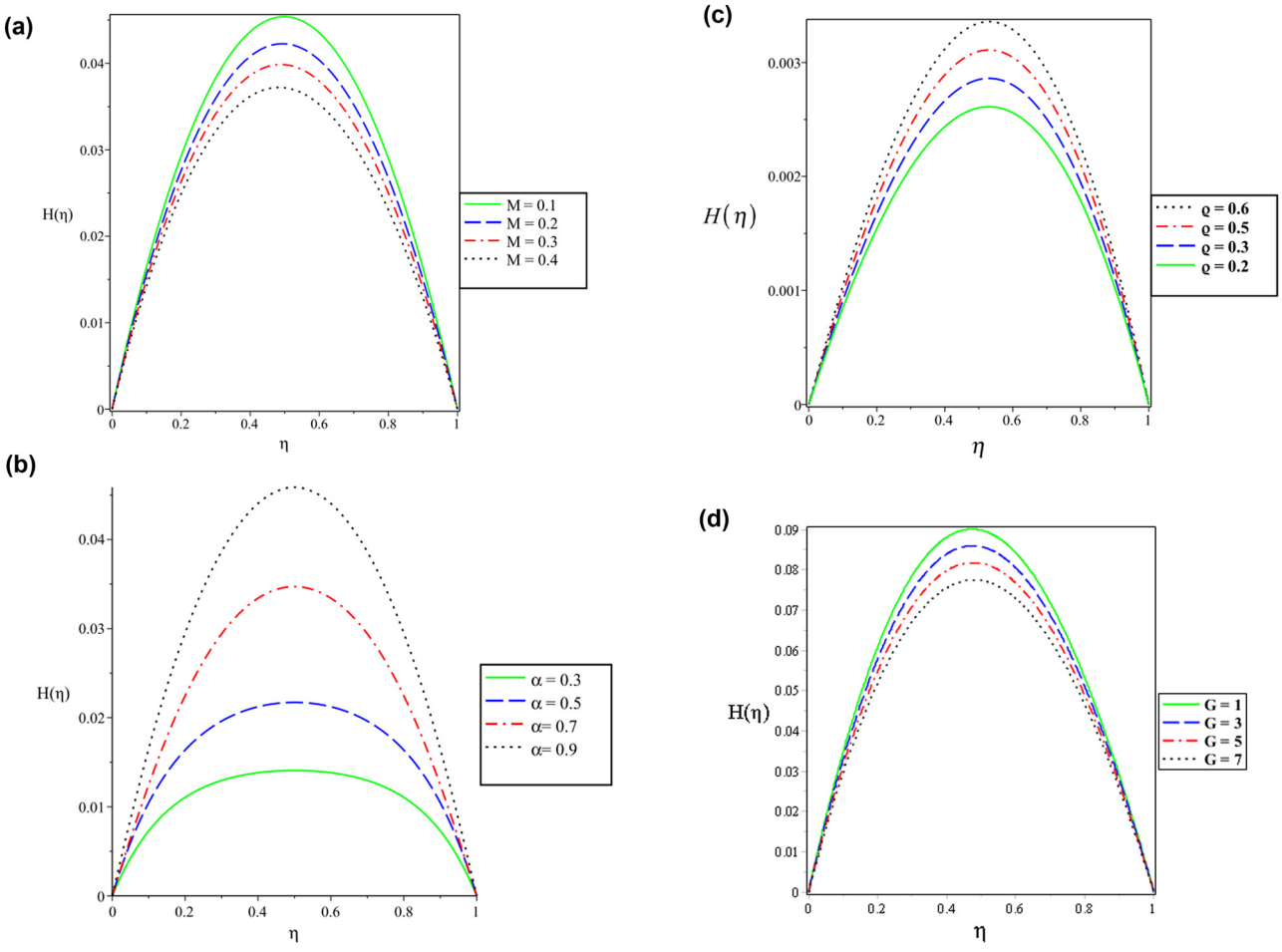

Figure 2: (a) Velocity distribution for increasing M. (b) Velocity distribution for increasing α. (c) Velocity distribution for increasing α. (d) Velocity distribution for increasing G.

5.4 Pressure gradient parameter (G)

Figure 2d shows how the flow of the Powell–Eyring fluid responds to increasing values of the G parameter. The reactive liquid experiences a reduction in the flow rate caused by the adverse influence of the pressure gradient. In the Couette device, pressure is exerted in the opposite direction of the flow. Therefore, the speed distribution is opposed by the force known as applied pressure, which acts in the inverse direction to the flow.

5.5 Frank–Kamenetskii (λ) and electric field loading (ϕ)

The Frank–Kamenetskii theory elucidates the phenomenon of thermal explosion in combustion. It focuses on the conditions where a uniform mixture of reactants is confined within a sealed container with walls at a constant temperature. The Brinkman number is the ratio of heat generated by viscous dissipation to heat carried by

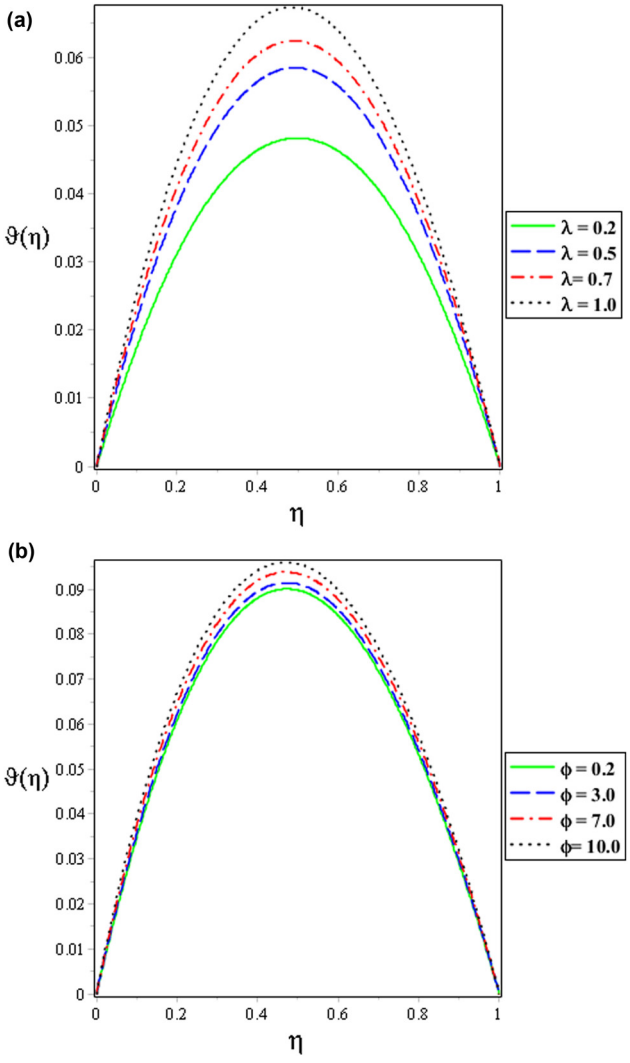

Figure 3: (a) The fluid temperature for increasing λ. (b) The fluid temperature for increasing ϕ.

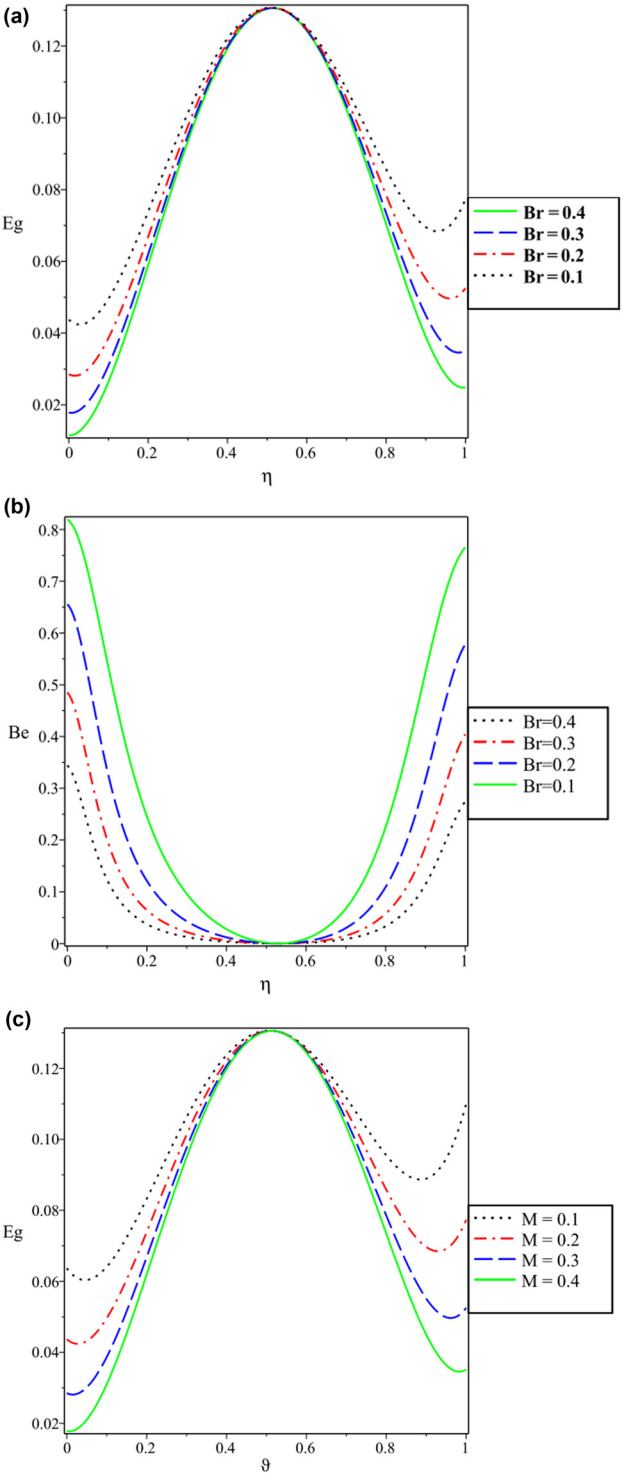

Figure 4: (a) E_g versus η for various Br. (b) Be versus η for various Br. (c) E_g versus η for various M.

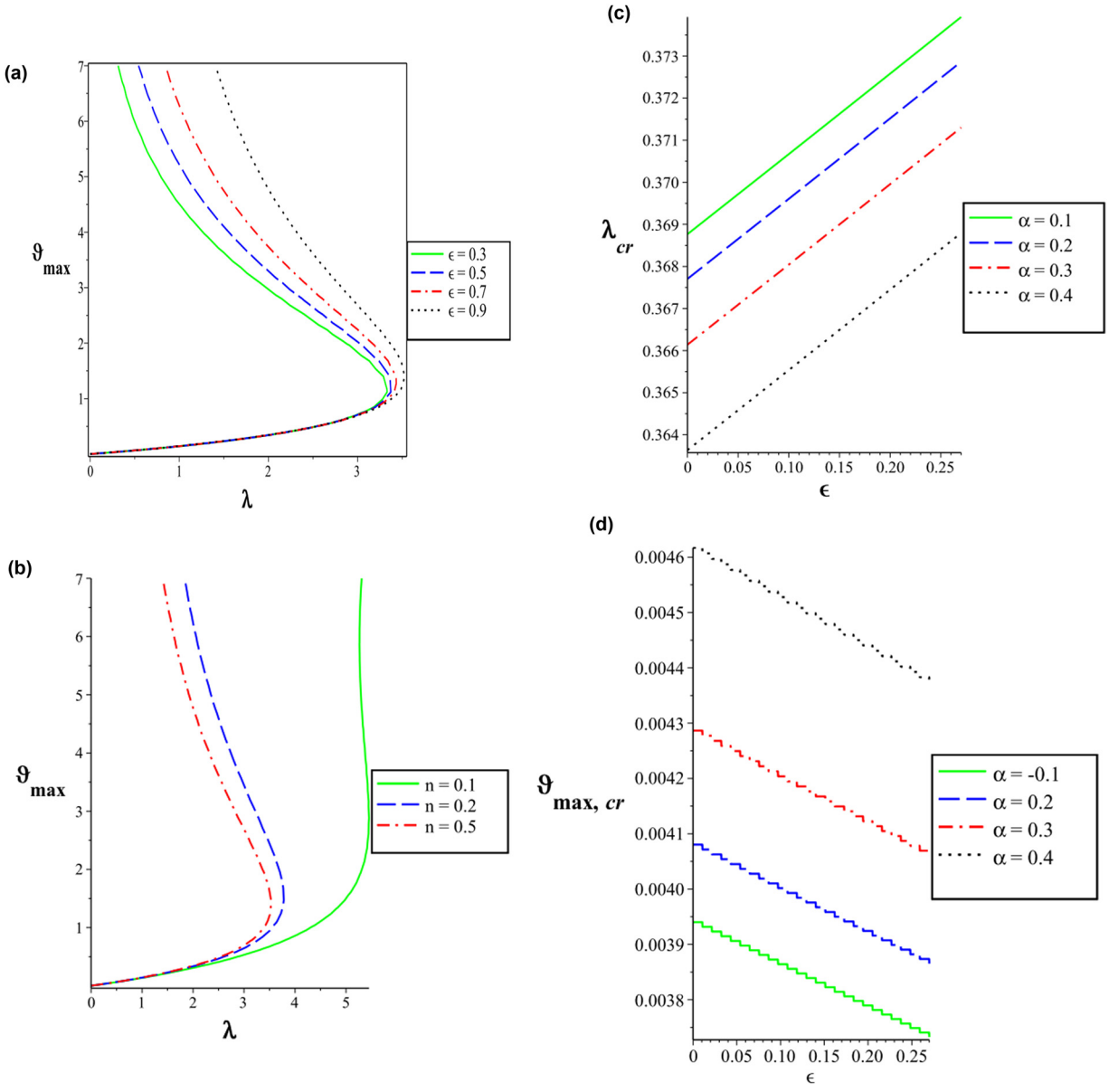

Figure 5: (a) Plot of criticality bifurcation versus λ for increasing ϵ. (b) Plot of criticality bifurcation against λ for increasing n. (c) λ_{cr} against ϵ for increasing α. (d) ϑ_{max} against ϵ for increasing α.

molecular conduction. Figure 3a shows how fluid temperature responds to changes in λ. The λ values are energetic heat sources; consequently, they both substantially increase the fluid temperature in an exothermic reaction. Figure 3b demonstrates how the fluid temperature responds when the fluid electric field loading is increased. An observation was made regarding an improvement in fluid temperature within the vertically oriented channel. The dragging force induced by the electric field loading in an electrically conducting fluid counteracts the heat generation components in the temperature equations.

5.6 Brinkman number (Br)

The major goal of this present research is to find approaches to lower the rate at which energy losses occur by taking into account the production of entropy when creating models to represent irreversible energy losses. To attain this objective, it is important to find factors that lead to an increase of disorder. Brinkman number (Br) signifies the evaluation between heat created due to internal friction and thermal transport via molecular conduction. Figure 4a demonstrates a consistent development in the creation of dimensionless E_g with Br, signifying a corresponding increase in E_g because of

viscous dissipation. The graph highlights an acceleration in the rate of non-dimensional generation at increased Br numbers, signifying the increasing significance of viscous dissipation as the fluid flow becomes more viscous. This observation is further reinforced by the rapid increase in the rate of non-dimensional generation as the Brinkman number increases. In real life, the Brinkman number displays how much thermal is created internally versus how much is transported externally. When it is high, heat moves more sluggishly via molecular conduction for the reason that more heat is created internally, leading to a larger increase in temperature. Bejan number tends to reach its peak in the central region of the channel, where the dominant factor causing irreversibility is heat transfer. The behavior (shown in Figure 4b) demonstrates a reduction in the Bejan number as Br number increases, indicating an increase in viscous dissipation irreversibility.

Figure 4c shows that as the value of the M increases, the profile of entropy production increases at the walls but declines towards the centerline of the channel. When a magnetic field interacts with a fluid in motion, it produces a force identified as the LF. The force works against the fluid's movement, causing more friction and energy loss. The system experiences an increase in entropy as the dissipated energy transforms into heat.

5.7 Solutions related to parameters for explosion and branch-chain bifurcation (BCB)

Figure 5a and b show the BCB diagrams corresponding to increasing values of λ and n within $(\epsilon, \vartheta_{max})$. The diagrams illustrate the maximum liquid heat (ϑ_{max}) and the λ parameter. For the term ϵ in the range of [0, 0.1], there exists a critical branch chain solution (λ_{cr}) for λ within the range of $0 \le \lambda \le \lambda_{cr}$. Therefore, two solutions are observed due to the nonlinear nature of the modeled equations. When $\lambda_{cr} < \lambda$, the thermal runaway is designated by the presence of both a stable lower branch solution and an unstable upper branch solution. Figure 5a and b illustrates variations in thermal runaway corresponding to increasing values of ϵ and n. The explosion effect occurred due to the finite-time attainment of infinite temperature.

Figure 5c and d demonstrates the variations in thermal criticality (λ_{cr}) and maximum energy (ϑ_{max}) and in response to changes in fluid variable viscosity (α). As the fluid variable viscosity increases, the magnitude of ϑ_{max} increases; however, λ_{cr} decreases. The figures show how changes in heat source terms affect the exothermic reaction in the fluid system.

5.8 Solutions related to parameters for the current density

Figure 6a and b illustrates how the current density is influenced by both the Frank–Kamenetskii term and the electric field loading. Both the Frank–Kamenetskii and the electric field significantly increase the current density at the channel walls by increasing the electric field conductivity within a hydromagnetic fluid flow. When the value of H = zero, it illustrates the distribution of fluid within a compact circuit configuration in the absence of an electric field.

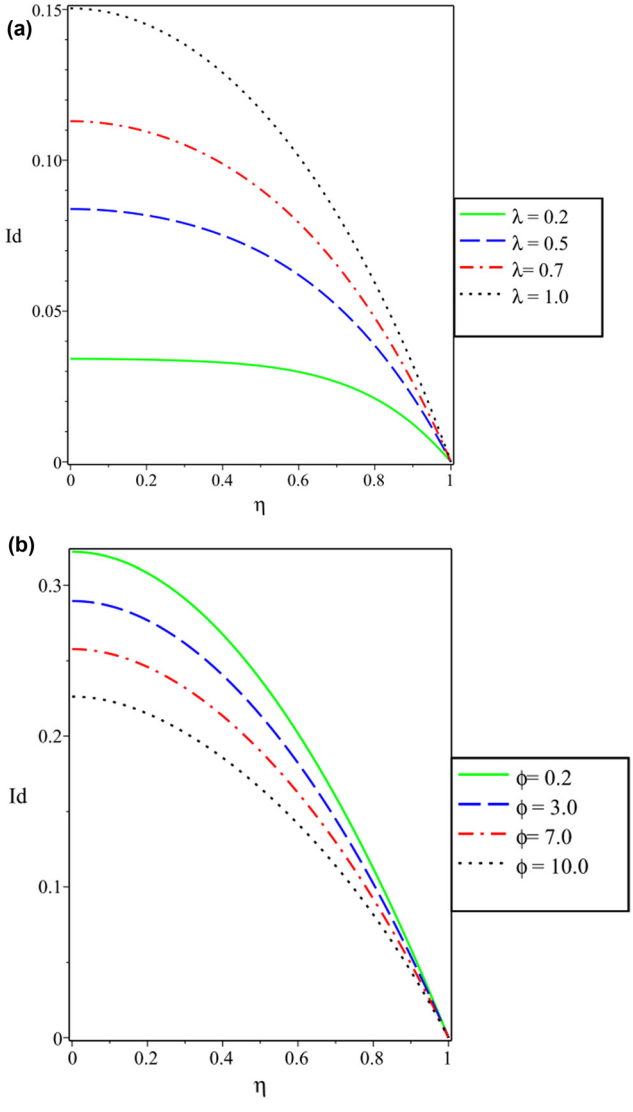

Figure 6: (a) Current density for various Frank–Kamenetskii terms. (b) The current density for various electric field loading.

6 Conclusions

The developed model describing the thermal runaway phenomena, electromagnetic control, and heat dynamics in the BCB of exothermic reactive flows under variable properties effects is considered. Numerical solutions are obtained using the SCS and Mathematica 11.3 software. The bifurcation exploration shows critical points where the system transitions from stable to unstable states, demonstrating conditions favorable for thermal runaway. The viscosity parameter positively influences the flow rate profile. The mounting strength of the magnetic field parameter resists the velocity distribution. The heat profile intensifies with a higher value of Frank–Kamenetskii and electric field loading. The entropy generation strengthens with a higher value of the Brinkman number. This understanding is vital for designing systems that aim to minimize energy loss and improve efficiency with an increase in the magnitude of the magnetic field and the speed distribution experiences an improvement.

Acknowledgement: The authors extend their appreciation to the Deanship of Scientific Research at the Islamic University of Madinah, Madinah, Saudi Arabia, for supporting this research work.

Author contributions: A.M.O. and H.G.: conceptualization, writing – original draft, methodology, software, formal analysis, and validation. A.O.A., A.A.U., and S.M.H: writing–original draft, data curation, investigation, visualization, and validation. U.K: conceptualization, writing – original draft, writing – review and editing, supervision, and validation. Y.Y., M.T., and N.N.: validation, investigation, writing – review and editing, formal analysis, project administration, and funding acquisition.

Conflict of interest: The authors declare no conflict of interest.

Ethical approval: No ethical research was conducted in this study.

Data availability statement: The datasets used and/or analyzed during the current study are available from the corresponding author upon reasonable request.

References

[1] Ghasemian A, Dinarvand S, Adamian A, Sheremet MA. Unsteady general three-dimensional stagnation point flow of a maxwell/Buongiorno non-Newtonian nanofluid. J Nanofluids. 2019;8(7):1544–59.

[2] Cocconi L, Garcia-Millan R, Zhen Z, Buturca B, Pruessner G. Entropy production in exactly solvable systems. Entropy. 2020;22:1252.

[3] Al-Kouz W, Owhaib W, Souayeh B, Hader M, Homod RZ. Cubic autocatalysis implementation in blood for non-Newtonian tetra hybrid nanofluid model through bounded artery. Appl Rheol. 2024;34:0007.

[4] Nasrin R, Alim MA. Entropy generation by nanofluid with variable thermal conductivity and viscosity in a flat plate solar collector. International Journal of Engineering. Sci Technol. 2015;7:80–93.

[5] Sharma BK, Kumar A, Gandhi R, Bhatti MM, Mishra NK. Entropy generation and thermal radiation analysis of EMHD Jeffrey nanofluid flow: Applications in solar energy. Nanomaterials. 2023;13:544.

[6] Ullah B, Khan U, Wahab HA, Khan I, Alam MN. Entropy generation analysis for MHD flow of hybrid nanofluids over a curved stretching surface with shape effects. J Nanomater. 2022;15:11–8.

[7] Obalalu AM, Ajala AO, Akindele AO, Areo OA, Ogundiran SD, Salaudeen KA, et al. Entropy generation minimization for radiative Casson fluid flow through permeable walls and convective heating: a comprehensive numerical investigation. Defect Diffus Forum. 2022;415:21–38.

[8] Din ZU, Ali A, De la Sen M, Zaman G. Entropy generation from convective–radiative moving exponential porous fins with variable thermal conductivity and internal heat generations. Sci Rep. 2022;12:1.

[9] Favas TK, Jilani G. Effect of variable thermal conductivity on entropy generation in a plate with internal energy generation. MATEC Web Conf. 2018;144:04001.

[10] Rikitu EH, Makinde OD. Entropy generation and heat transfer analysis of Eyring-Powell nanofluid flow through inclined microchannel subjected to magnetohydrodynamics and heat generation. Int J Thermofluids. 2024;22:100640.

[11] Zaib A, Rashidi MM, Chamkha AJ. Flow of Nanofluid containing gyrotactic microorganisms over static wedge in darcy-brinkman porous medium with convective boundary condition. J Porous Media. 2018;21(10):911–28.

[12] Abbas M, Khan N, Hashmi MS, Alhefthi RK, Rezapour S, Inc M. Thermal Marangoni convection in two-phase quadratic convective flow of dusty MHD trihybrid nanofluid with non-linear heat source. Case Stud Therm Eng. 2023;57:104190.

[13] Waqas H, Farooq U, Naseem R, Hussain S, Alghamdi M. Impact of MHD radiative flow of hybrid nanofluid over a rotating disk. Case Stud Term Eng. 2021;26:101015.

[14] Lone SA, Khan A, Raiza Z, Alrabaiah H, Shahab S, Saeed A, et al. A semi-analytical Solut magnetohydrodynamic blood-based ternary hybrid nanofluid flow a convectively heated bidirectional stretching Surf velocity slip Cond. AIP Adv. 2024;14:4.

[15] Tabrez M, Khan WA. Exploring physical aspects of viscous dissipation and magnetic dipole for ferromagnetic polymer nanofluid flow. Waves Random Complex Media. 2021;1–20.

[16] Shah Z, Dawar A, Islam S. Influence of Brownian motion and thermophoresis parameters on silver-based di-hydrogen CNTs between two stretchable rotating disks. Phys Scr. 2021;96(5):055205.

[17] Khan WA. Impact of time-dependent heat and mass transfer phenomenon for magnetized Sutterby nanofluid flow. Waves Random Complex Media. 2022;1–15.

[18] Punith Gowda RJ, Naveen Kumar R, Jyothi AM, Prasannakumara BC, Sarris IE. Impact of binary chemical reaction and activation energy on heat and mass transfer of Marangoni driven boundary layer flow of a non-Newtonian nanofluid. Processes. 2021;9(4):702.
[19] Kareem SO, Adesanya SO, Vincent UE. Second law analysis for hydromagnetic couple stress fluid flow through a porous channel. Alex Eng J. 2020;55:925–31.
[20] Algehyne EA, Abdelmohsen SAM, Gowda RJP, Kumar RN, Abdelbacki AMM, Gorji MR, et al. Mathematical modeling of magnetic dipole effect on convective heat transfer in Maxwell nanofluid flow: single and multi-walled carbon nanotubes. Waves Random Complex Media. 2023;33:489–504.
[21] Madhu M, Kishan N, Chamkha AJ. Unsteady flow of a maxwell nanofluid over a stretching surface in the presence of magneto-hydrodynamic and thermal radiation effects. Propul Power Res. 2017;6(1):31–40.
[22] Feng S, Chen Q. Analysis on non-Newtonian characteristics for nano magnetic fluid. Procedia Eng. 2017;174:1208–14.
[23] Hussain Z, Aljuaydi F, Ayaz M, Islam S. Enhancing thermal efficiency in MHD kerosene oil-based ternary hybrid nanofluid flow over a stretching sheet with convective boundary conditions. Results Eng. 2024;22:102151.
[24] Iqbal J, Abbasi FM, Nawaz R. Numerical investigation of magneto-hydrodynamic bioconvection peristalsis of Powell–Eyring nanofluid. Numer Heat Transf, Part A: Appl. 2024;22:1–22.
[25] Khan AA, Fatima G, Sait SM, Ellahi R. Electromagnetic effects on two-layer peristalsis flow of Powell–Eyring nanofluid in axisymmetric channel. J Therm Anal Calorim. 2024;1498:3631–44.
[26] Vijatha M, Bala Anki Reddy P. Second law analysis on magnetohydrodynamics flow of Eyring-Powell hybrid nanofluid over a cylinder/plate with non-linear thermal radiation and Cattaneo-Christov heat flux: Numerical and semi-analytical simulations. Numer Heat Transf, Part B: Fundam. 2024;30:1–29.
[27] Allehiany FM, Riaz A, Alfwzan WF, Shaheen S, Muhammad T. Cilia flow of magnetized Eyring-Powell nanofluid in a vertical thermal channel with viscous dissipation: An application of Adomian decomposition method. Ain Shams Eng J. 2024;15(5):102699.
[28] Hussain A, Mao Z. Heat transfer analysis of MHD Prandtl-Eyring fluid flow with Christov-Cattaneo heat flux model. Numer Heat Transf, Part A: Appl. 2024;8:1–21.
[29] Nisar Z, Ahmed B, Aziz A, Muhammad K, Elseesy IE. Impacts of entropy generation for nonlinear radiative peristaltic transport of Powell-Eyring nanofluid: a numerical study. Numerical Heat Transfer. Part A: Appl. 2023;24:1–9.
[30] Mondal SK, Pal D. Significance of binary chemical reaction with activation energy in magneto-bioconvection flow of a Powell Eyring nanofluid past an inclined stretching sheet by considering temperature-dependent viscosity and thermal conductivity. Int J Model Simul. 2023;1–9.
[31] Nadeem S, Mushtaq A, Alzabut J, Ghazwani HA, Eldin SM. The flow of an Eyring Powell Nanofluid in a porous peristaltic channel through a porous medium. Sci Rep. 2023 Jun;13:9694.
[32] Hussain Z, Khan WA, Ali M, Muhammad T, Liu H, Waqas M. Significance of chemically reactive magnetized Eyring-Powell nanofluid flow comprising gyrotactic moment of microorganism and radiative analysis. J Magn Magn Mater. 2023;581:170955.
[33] Ibrahim W, Lamesse T. Powell-Eyring nanofluid analysis with finite element method when past stretching sheet with convective heating and passive control of nanoparticle. Int J Thermofields. 2023;19:100388.
[34] Shah NA, Koriko OK, Ramesh K, Oreyeni T. Rheology of bioconvective stratified Eyring-Powell nanofluid over a surface with variable thickness and homogeneous-heterogeneous reactions. Biomass Convers Biorefin. 2023;13:1–7.
[35] Salawu SO, Hassan AR, Abolarinwa A, Oladejo NK. Thermal stability and entropy generation of unsteady reactive hydromagnetic Powell-Eyring fluid with variable electrical and thermal conductivities. Alex Eng J. 2019;58:519–29.
[36] Chamkha AJ. Non-Darcy fully developed mixed convection in a porous medium channel with heat generation/absorption and hydromagnetic effects. Numer Heat Transf, Part A Appl. 1997;1:653–75.
[37] Kumar A, Sharma BK, Bin-Mohsen B, Fernandez-Gamiz U. Statistical analysis of radiative solar trough collectors for MHD Jeffrey hybrid nanofluid flow with gyrotactic microorganism: entropy generation optimization. Int J Numer Methods Heat Fluid Flow. 2024;23:948–79.
[38] Salawu SO, Fatunmbi EO, Okoya SS. MHD heat and mass transport of Maxwell Arrhenius kinetic nanofluid flow over stretching surface with nonlinear variable properties. Results Chem. 2023;3:100125.